Eur. Phys. J. B **51**, 425–433 (2006)
DOI: 10.1140/epjb/e2006-00245-3

THE EUROPEAN PHYSICAL JOURNAL B

Charge and spin currents tunnelling through a toroidal carbon nanotube side-coupled with a quantum dot

H.-K. Zhao[1,2,3,a], J. Wang[2], and Q. Wang[3]

[1] CCAST (World Laboratory), P.O. Box 8730, Beijing 100080, P.R. China
[2] Department of Physics, The University of Hong Kong, Pokfulam Road, Hong Kong, P.R. China
[3] Department of Physics, Beijing Institute of Technology, Beijing 100081, P.R. China

Received 25 March 2006
Published online 21 June 2006 –

Abstract. We have investigated the mesoscopic transport through the system with a quantum dot (QD) side-coupled to a toroidal carbon nanotube (TCN) in the presence of spin-flip effect. The coupled QD contributes to the mesoscopic transport significantly through adjusting the gate voltage and Zeeman field applied to the QD. The compound TCN-QD microstructure is related to the separate subsystems, the applied external magnetic fields, as well as the combination of subsystems. The spin current component I_z^s is independent on time, while the spin current components I_x^s and I_y^s evolve with time sinusoidally. The rotating magnetic field induces novel levels due to the spin splitting and photon absorption procedures. The suppression and enhancement of resonant peaks, and semiconductor-metal phase transition are observed by studying the differential conductance through tuning the source-drain bias and photon energy. The magnetic flux induces Aharonov-Bohm oscillation, and it controls the tunnelling behavior due to adjusting the flux. The Fano type of multi-resonant behaviors are displayed in the conductance structures by adjusting the gate voltage V_g and the Zeeman field $\mathbf{B}_2$ applied to the QD.

PACS. 85.35.-p Nanoelectronic devices – 73.23.-b Electronic transport in mesoscopic systems – 72.25.Mk Spin transport through interfaces – 73.21.La Quantum dots

1 Introduction

The research on electron transport through hybrid device structures is presented for the new stage of investigation, in which the carbon devices are coupled to different materials [1–3]. The toroidal carbon nanotube (TCN) is a form of carbon structure, which is a torus structure by bending the carbon tube such that the two edges are connected [4–7]. The TCN is formed by rolling a finite graphite sheet from the origin to the vectors $\mathbf{R}_x$ and $\mathbf{R}_y$ simultaneously, and it is denoted by $(m_1, m_2; p_1, p_2)$ as convention. Two kinds of TCN with highly symmetric structures are armchair $(m, m; -p, p)$ TCN and zigzag $(m, 0; -p, 2p)$ TCN. The armchair TCN possesses the symmetry with armchair structure along the transverse direction and zigzag structure along the longitudinal direction. The zigzag TCN has the structure in both of the directions being zigzag. In the absence of magnetic flux, the armchair TCN is a metal as $p = 3\nu$ (type I TCN), while it is a semiconductor with narrow energy gap as $p = 3\nu \pm 1$ (type II TCN) where ν is an integer. For the zigzag TCN in the absence of magnetic flux, there exists large energy gap as $m \neq 3\nu$ (type III TCN). There is no technique question for the fabrication of TCNs from single-wall carbon nanotubes (SWCNs) [7,8]. The combination of terminal structures and TCN together forms coupled density of state (DOS), and the tunnelling current is determined by the detailed constructions [9–11]. One of the most important applications of carbon nanotubes is to serve the molecular samples as a kind of spin devices. For instance, the spin coherent field effect transistor proposed associated with the spin precession due to the spin-orbit coupling in narrow-gap semiconductors [12]. The experiments on the control and manipulation of spin made it possible for the application of spintronic nano-devices [13,14]. The theoretical works on the spin-current circuit and generator phenomena, such as spin-battery proposals [15,16], and the spin field effect transistor (SFET) [17] are also proposed to develop the spintronics. Recently, we have made the contributions to the development of spintronics in the aspects for investigating the spin-flip mesoscopic transport through a quantum dot (QD) responded by a rotating and an oscillating magnetic fields [18]; the spin and charge currents tunnelling through a coupled TCN system in the presence of rotating magnetic field and an Aharonov-Bohm magnetic flux [19]; the system consisting of a central QD and two SWCN leads [20]. Many novel properties are revealed relating to the material structures.

As a QD is coupled to a mesoscopic ring, the charge of a single electron transferring from one mesoscopic region

[a] e-mail: zhaohonk@yahoo.com

to another can alter the mesoscopic properties drastically. The polarized charge transfer in an external capacitive circuit causes the changing of potential landscape, and it changes the phase-sensitive properties of the mesoscopic sample [21]. It is significant to study the transport behaviors of electronic charge and spin tunnelling through the mesoscopic system with a quantum dot coupled to a ring-like sample. In this paper, we investigate the mesoscopic transport through a coupled TCN-QD system in the presence of spin-flip effect. A QD is side-coupled with a TCN, and the TCN is connected to two normal metal leads. A rotating magnetic field is applied to the TCN to induce spin-dependent tunnelling, which acts as spin generator in the TCN. An static magnetic field is applied to produce a magnetic flux threaded through the TCN. This magnetic flux induces Aharonov-Bohm oscillation, and it controls the tunnelling behavior due to adjusting the flux. We consider the system of TCN with the diameter ratio of the tube to the ring as $d_t/D_t \ll 1$. The QD is applied with gate voltage, and the terminals are applied with source-drain bias voltage. The detailed structure of compound TCN-QD dedicates important contribution to the spin-flip mesoscopic transport.

2 Hamiltonian and formalism

We consider the system that the TCN is exposed to the rotating magnetic field $\mathbf{B}_0(\mathrm{t}) = B_0[\sin\theta\cos(\omega\mathrm{t})\mathbf{e}_x + \sin\theta\sin(\omega t)\mathbf{e}_y + \cos\theta\mathbf{e}_z]$, where ω is angular frequency, and θ is tilt angle between the z-axis and rotating magnetic field. This kind of magnetic field is used to produce pure spin current in a quantum dot system in references [17,22]. We restrict this field so that there is no magnetic flux threaded through the TCN. Another static magnetic field $\mathbf{B}_1$ is applied in $\mathbf{e}_z$ direction, which produces a static magnetic flux ϕ threaded through the TCN. The static magnetic field $\mathbf{B}_1$ does not applied on the ring, but only produces an Aharonov-Bohm magnetic flux. The magnetic field $\mathbf{B}_0(\mathrm{t})$ is screened in order not to affect the leads. The side-coupled quantum dot is applied with a gate voltage V_g to control the mesoscopic transport by tuning V_g. The schematic diagram of this system is similar to Figure 1 in reference [19] to help understanding our geometric structure, but there is no coupled QD in that paper. The QD is a mesoscopic system, however, it can be served as a mesoscopic electron reservoir, and electron can transport between TCN and QD. If the chemical potentials between the terminals and QD are not equal, the charge and spin currents may exist in the terminals and QD. The rotating field applies a magnetic field with maximum magnitude of the field on the ring, and the magnetic field varies with the angles θ, and $\varphi(t) = \omega t$. At a definite time, the effective field for electrons in the TCN is different site by site with respect to θ due to the geometric structure of TCN [23]. The variation of the magnetic field $\Delta\mathbf{B}_0(\mathrm{t})$ is proportional to $\Delta\theta < d_t/D_t \ll 1$. Thus, the difference of magnetic field on the TCN associated with θ can be neglected obviously for our system. Generally, We apply a Zeeman field $\mathbf{B}_2$ on the QD to serve as a magnetic controlling field, which is not necessary to be supplied simultaneous with the other fields. The Zeeman field $\mathbf{B}_2$ has different contributions compared with the rotating magnetic field.

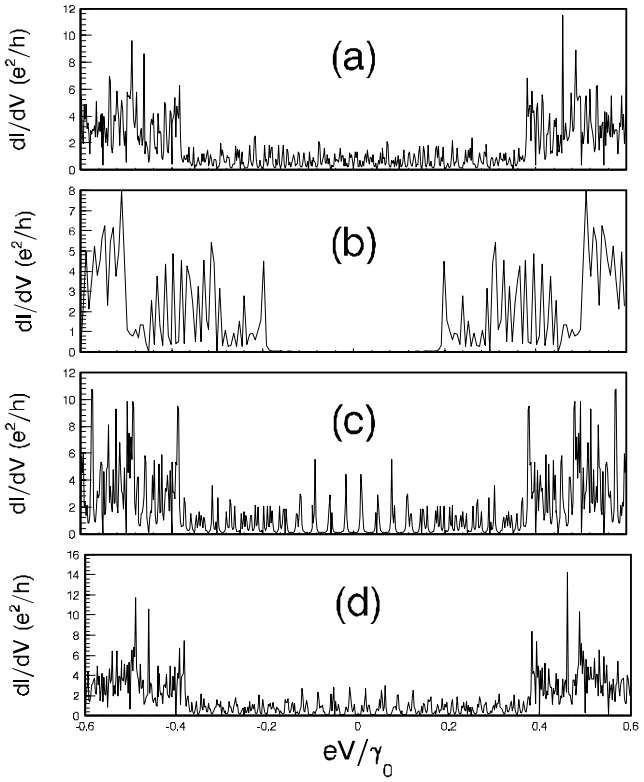

Fig. 1. The differential conductance dI/dV versus source-drain bias eV. The parameters are chosen as $\phi = 0$, $V_g = 0$, $B_2 = 0, \theta = \pi/3$, $\mathcal{N} = 30$. Diagram (a) is related to the (7, 7; −160, 160) TCN as $\hbar\omega = 0.01\gamma_0$; diagram (b) is related to the (7, 0; −160, 320) TCN as $\hbar\omega = 0$; diagrams (c) and (d) correspond to the (7, 7; −159, 159) TCN as $\hbar\omega = 0$, and $\hbar\omega = 0.01\gamma_0$, respectively.

The central TCN is described by tight-binding Hamiltonian, and the two normal metal leads are described by the free electron systems. The QD is relatively large characterized by multi-level free electron model. We consider the situation that the leads broaden immediately at the connections to the TCN, and they are large enough to be considered as equilibrium macroscopic electron reservoirs. In the diagonal representation of TCN, the electronic properties can be determined by the total Hamiltonian

$$H = \sum_{k\sigma}\sum_{\gamma\in\{L,R\}} \epsilon_{\gamma,k\sigma} a^\dagger_{\gamma,k\sigma} a_{\gamma,k\sigma} + \sum_{j\ell\delta\sigma} E_{\delta,j\ell}(\phi) c^\dagger_{\delta\sigma,j\ell} c_{\delta\sigma,j\ell} + \sum_{\ell\sigma} E_{d,\ell\sigma} d^\dagger_{\ell\sigma} d_{\ell\sigma} + \sum_{j\ell\delta}\Bigg\{ \sum_{\sigma\sigma'} c^\dagger_{\delta\sigma,j\ell}\Omega_{\sigma\sigma'}(t) c_{\delta\sigma',j\ell} + \sum_{k\sigma}\sum_{\gamma\in\{L,R\}} \left[R^*_{\gamma\delta,j\ell}(k) c^\dagger_{\delta\sigma,j\ell} a_{\gamma,k\sigma} + \mathrm{H.c.}\right] + \sum_{\ell'\sigma}\left[T^{\ell'\sigma *}_{\delta,j\ell} c^\dagger_{\delta\sigma,j\ell} d_{\ell'\sigma} + \mathrm{H.c.}\right]\Bigg\}. \quad (1)$$

In the Hamiltonian (1), $a^{\dagger}_{\gamma,k\sigma}$ ($a_{\gamma,k\sigma}$), $c^{\dagger}_{\delta\sigma,j\ell}$ ($c_{\delta\sigma,j\ell}$), and $d^{\dagger}_{\ell\sigma}$ ($d_{\ell\sigma}$) are the creation (annihilation) operators of electrons in the two leads, TCN and QD respectively. $E_{d,\ell\sigma}$ is the energy level of QD defined by $E_{d,\ell\sigma} = E_{d\ell} + eV_g + \lambda_\sigma \mu B_2$. Here $R_{\gamma\delta,j\ell}(k)$ is interaction strength of electrons between the γth lead and TCN. The quantity $T^{\ell'\sigma}_{\delta,j\ell}$ is the interaction strength of electrons between the QD and TCN. $\Omega_{\sigma\sigma'}(t)$ are elements of the matrix $\mathbf{\Omega}$(t) in spin space defined as

$$\mathbf{\Omega}(\mathrm{t}) = \mu \mathrm{B}_0 \begin{pmatrix} \cos\theta, & \sin\theta\, e^{-i\omega t} \\ \sin\theta\, e^{i\omega t}, & -\cos\theta \end{pmatrix}, \tag{2}$$

where $\mu = g\mu_B/2$ is magnetic moment of electron, μ_B is the Bohr magneton, g is Lande factor which is approximately equal to 2. The energy of TCN is intimately associated with the structure of concrete TCN. The energy level $E_{\delta,j\ell}(\phi)$ of armchair TCN in the tight-binding approximation is given by [8]

$$E_{\delta,j\ell}(\phi) = \delta\gamma_0 \Bigg\{ 1 + 4\cos\left(\frac{\pi j}{m}\right)\cos\left[\frac{\pi(\ell+\phi/\phi_0)}{p}\right] + 4\cos^2\left[\frac{\pi(\ell+\phi/\phi_0)}{p}\right] \Bigg\}^{1/2}, \tag{3}$$

and the energy level of the zigzag TCN in the tight-binding approximation is given by

$$E_{\delta,j\ell}(\phi) = \delta\gamma_0 \Bigg\{ 1 + 4\cos\left(\frac{\pi j}{m}\right)\cos\left[\frac{\pi(\ell+\phi/\phi_0)}{p}\right] + 4\cos^2\left(\frac{\pi j}{m}\right) \Bigg\}^{1/2}, \tag{4}$$

where $j = 1, 2, ..., m; \ell = 1, 2, ..., 2p; \delta = \pm$, $\gamma_0 = 3.033$ eV, and $\phi_0 = h/e$ is the flux quantum. The upper half of the energy dispersion curves describes the π^*-energy antibonding band (unoccupied state), and the lower half of it is the π-energy bonding band (occupied state). We take the chemical potential of the right lead as the reference of energy measurement to ensure $\mu_L - \mu_R = eV$, where V is the voltage between the two leads.

In order to derive the tunnelling current by the nonequilibrium Green's function technique [24,25], we define the retarded (advanced) Green's function of the coupled TCN as

$$G^{r(a)}_{\delta j\ell,\sigma\sigma'}(t,t') = \mp\frac{i}{\hbar}\theta(\pm t \mp t')\langle[c_{\delta\sigma,j\ell}(t), c^{\dagger}_{\delta\sigma',j\ell}(t')]_+\rangle, \tag{5}$$

and the Keldysh Green's function of the coupled TCN as

$$G^{<}_{\delta j\ell,\sigma\sigma'}(t,t') = \frac{i}{\hbar}\langle c^{\dagger}_{\delta\sigma',j\ell}(t') c_{\delta\sigma,j\ell}(t)\rangle. \tag{6}$$

The spin operator of a lead is defined by $\hat{\mathbf{S}}_{\gamma,\mu\nu} = \sum_k a^{\dagger}_{\gamma,k\mu} a_{\gamma,k\nu} \mathbf{s}_{\mu\nu}$, and the QD is $\hat{\mathbf{S}}_{d,\mu\nu} = \sum_\ell d^{\dagger}_{\ell\mu} d_{\ell\nu} \mathbf{s}_{\mu\nu}$, where $\mathbf{s}_{\mu\nu} = \frac{\hbar}{2}\boldsymbol{\sigma}_{\mu\nu}$ is the spin angular moment of electron. The spin current components are determined by the continuity equation of the spin operator as $\partial\hat{\mathbf{S}}_{\gamma,\mu\nu}/\partial t + \hat{I}_{\gamma,\mu\nu}(t)\mathbf{s}_{\mu\nu} = 0$. The current components of the γth lead are obtained by taking ensemble expectation and quantum average to give

$$I_{\gamma,\mu\nu}(t) = \sum_{\ell j\delta}\int dt_1 \big\{ G^r_{\delta j\ell,\nu\mu}(t,t_1)\Sigma^<_{\gamma\delta,j\ell\mu}(t_1,t) + G^<_{\delta j\ell,\nu\mu}(t,t_1)\Sigma^a_{\gamma\delta,j\ell\mu}(t_1,t) - [\Sigma^r_{\gamma\delta,j\ell\nu}(t,t_1)G^<_{\delta j\ell,\nu\mu}(t_1,t) + \Sigma^<_{\gamma\delta,j\ell\nu}(t,t_1)G^a_{\delta j\ell,\nu\mu}(t_1,t)]\big\}, \tag{7}$$

for $\gamma \in \{L, R, d\}$. This is a general expression for the spin current components containing the diagonal and off-diagonal elements in spin space. The diagonal elements in spin space are related to charge transport, and spin transport of the $\mathbf{s}^z$ component. The off-diagonal current elements in spin space are associated with the spin transport of $\mathbf{s}^x$ and $\mathbf{s}^y$ components. The self-energies $\Sigma^X_{\gamma\delta,j\ell\nu}(t,t')$ signifies that $\Sigma^X_{\gamma\delta,j\ell\nu}(t,t') = \sum_k |R_{\gamma\delta,j\ell}(k)|^2 g^X_{\gamma,k\nu}(t,t')$ as $\gamma \in \{L,R\}$, and $\Sigma^X_{d\delta,j\ell\sigma}(t,t') = \sum_{\ell'} |T^{\ell'\sigma}_{\delta,j\ell}|^2 g^X_{d,\ell'\sigma}(t,t')$ as $\gamma = d$, where $g^X_{\gamma,k\nu}(t,t')$ and $g^X_{d,\ell'\sigma}(t,t')$ are the isolated Green's functions of the leads and QD. The symbol $X \in \{r, a, <\}$ denotes the retarded, advanced, and Keldysh Green's functions and corresponding self-energies of leads and QD. The spin current components can be expressed by the Fourier transformed Green's functions and self-energies as

$$I_{\gamma,\mu\nu}(t) = \frac{1}{h}\sum_{\ell j\delta}\int d\epsilon_1 d\epsilon_2 e^{\frac{i}{\hbar}\epsilon_{21}t}\Big\{ G^r_{\delta j\ell,\nu\mu}(\epsilon_1,\epsilon_2)\Sigma^<_{\gamma\delta,j\ell\mu}(\epsilon_2) + G^<_{\delta j\ell,\nu\mu}(\epsilon_1,\epsilon_2)\Sigma^a_{\gamma\delta,j\ell\mu}(\epsilon_2) - \big[\Sigma^r_{\gamma\delta,j\ell\nu}(\epsilon_1)G^<_{\delta j\ell,\nu\mu}(\epsilon_1,\epsilon_2) + \Sigma^<_{\gamma\delta,j\ell\nu}(\epsilon_1)G^a_{\delta j\ell,\nu\mu}(\epsilon_1,\epsilon_2)\big]\Big\}, \tag{8}$$

where $\epsilon_{21} = \epsilon_2 - \epsilon_1$ and $G^X_{\delta j\ell,\nu\mu}(\epsilon_1,\epsilon_2)$, $(X \in \{r, a, <\})$, are the Fourier transformed retarded, advanced, and Keldysh Green's functions of the coupled TCN. $\Sigma^X_{\gamma\delta,j\ell\nu}(\epsilon)$ are the Fourier transformed self-energies of $\Sigma^X_{\gamma\delta,j\ell\nu}(t,t')$ determined by $\Sigma^X_{\gamma\delta,j\ell\nu}(\epsilon) = \sum_{k\gamma} |R_{\gamma\delta,j\ell}(k)|^2 g^X_{\gamma,k\sigma}(\epsilon)$, and $\Sigma^X_{d\delta,j\ell\sigma}(\epsilon) = \sum_{\ell'} |T^{\ell'\sigma}_{\delta,j\ell}|^2 g^X_{d,\ell'\sigma}(\epsilon)$ where $g^X_{\gamma,k\sigma}(\epsilon)$ and $g^X_{d,\ell'\sigma}(\epsilon)$ are the Green's functions of the γth lead and QD, respectively. The retarded (advanced) and Keldysh Green's functions of leads are $g^{r(a)}_{\gamma,k\sigma}(\epsilon) = 1/[\epsilon - \epsilon_{\gamma,k\sigma} \pm i\eta]$,$(\eta \to +0)$, and $g^<_{\gamma,k\sigma}(\epsilon) = 2\pi i f_\gamma(\epsilon)\delta(\epsilon - \epsilon_{\gamma,k\sigma})$. The corresponding Green's functions of the QD are determined by $g^{r(a)}_{d,\ell\sigma}(\epsilon) = 1/[\epsilon - E_{d,\ell\sigma} \pm i\eta]$, and $g^<_{d,\ell\sigma}(\epsilon) = 2\pi i f_d(\epsilon)\delta(\epsilon - E_{d,\ell\sigma})$. The Fermi distribution function of the leads and QD are given by $f_\gamma(\epsilon) = 1/\{\exp[(\epsilon - \mu_\gamma)/K_BT] + 1\}$, for $\gamma \in \{L, R, d\}$, where K_B is the Boltzmman constant. The density of state (DOS) of the leads $\rho_{\gamma\sigma}(\epsilon) = \sum_k \delta(\epsilon - \epsilon_{\gamma,k\sigma})$ can be expressed by a function with continuous energy of the incident electrons. However, the DOS of isolated QD is determined by its discrete energy levels $E_{d,\ell\sigma}$ as $\rho_{d\sigma}(\epsilon) = \sum_\ell \delta(\epsilon - E_{d,\ell\sigma})$.

From the Dyson-like equation, one can obtain the retarded Green's function in the Fourier space as

$$G^r_{\delta j\ell,\sigma\sigma'}(\epsilon,\epsilon') = G^r_{\delta j\ell,\sigma\sigma}(\epsilon)[\delta(\epsilon-\epsilon')\delta_{\sigma\sigma'} + \gamma(\theta)\tilde{g}^r_{\delta j\ell,\bar{\sigma}\bar{\sigma}}(\tilde{\epsilon}_\sigma)\delta(\tilde{\epsilon}_\sigma-\epsilon')\delta_{\bar{\sigma}\sigma'}], \quad (9)$$

where $\tilde{g}^r_{\delta j\ell,\sigma\sigma}(\epsilon) = 1/[\epsilon - \varepsilon_{\delta j\ell,\sigma}(\theta) - \tilde{\Sigma}^r_{\delta j\ell,\sigma}(\epsilon)]$, and $\varepsilon_{\delta j\ell,\sigma}(\theta) = E_{\delta,j\ell}(\phi) + \lambda_\sigma \mu B_0 \cos\theta$. The self-energy $\tilde{\Sigma}^r_{\delta j\ell,\sigma}(\epsilon)$ of the coupled system is defined by the summation of Fourier transformed self-energies of leads and quantum dot as $\tilde{\Sigma}^r_{\delta j\ell,\sigma}(\epsilon) = \sum_{\gamma\in\{L,R,d\}} \Sigma^r_{\gamma\delta,j\ell\sigma}(\epsilon)$. In the formulas we have used the notations as $\gamma(\theta) = \mu B_0 \sin\theta$, $\tilde{\epsilon}_\sigma = \epsilon - \lambda_\sigma \hbar\omega$, where λ_σ is the eigenvalue of the Pauli operator σ_z, for $\lambda_\uparrow = 1, \lambda_\downarrow = -1$. The diagonal elements of the retarded Green's function in spin space is derived to be

$$G^r_{\delta j\ell,\sigma\sigma}(\epsilon) = \frac{\tilde{g}^r_{\delta j\ell,\sigma\sigma}(\epsilon)}{1-\gamma(\theta)^2\tilde{g}^r_{\delta j\ell,\sigma\sigma}(\epsilon)\tilde{g}^r_{\delta j\ell,\bar{\sigma}\bar{\sigma}}(\tilde{\epsilon}_\sigma)}. \quad (10)$$

The second term in equation (9) contributes to the spin-flip off-diagonal mesoscopic transport current components. The diagonal elements of the Green's function given in equation (10) also contains the spin-flip effect which is related to the term of $\gamma(\theta)$ in the denominator. As $\theta = 0$ the system is associated with the situation that the rotating magnetic field reduces to the constant Zeeman field $\mathbf{B}_0 = \mathrm{B}_0\mathbf{e}_z$ applying to the TCN, and there is no spin-flip effect.

The Keldysh Green's function of the coupled TCN can be derived similarly from the Dyson-like equation as

$$G^<_{\delta j\ell,\sigma\sigma'}(\epsilon,\epsilon') = G^r_{\delta j\ell,\sigma\sigma}(\epsilon)[\tilde{\Sigma}^<_{\delta j\ell,\sigma}(\epsilon)G^a_{\delta j\ell,\sigma\sigma'}(\epsilon,\epsilon') + \gamma(\theta)\tilde{g}^r_{\delta j\ell,\bar{\sigma}\bar{\sigma}}(\tilde{\epsilon}_\sigma)\tilde{\Sigma}^<_{\delta j\ell,\bar{\sigma}}(\tilde{\epsilon}_\sigma)G^a_{\delta j\ell,\bar{\sigma}\sigma'}(\tilde{\epsilon}_\sigma,\epsilon')]. \quad (11)$$

Equation (9–11) contain all the information of the charge and spin transport, such as the spin diagonal and spin off-diagonal transport, the time-dependent situation caused by the rotating field, and the resonant charge tunnelling through the compound band structure of TCN-QD. The explicit time-dependent current evolution is presented by substituting the Green's functions given in equations (9) and (11) into equation (8). The Green's functions can be expressed generally in the form

$$G^X_{\delta j\ell,\sigma\sigma'}(\epsilon,\epsilon') = G^X_{\delta j\ell,\sigma\sigma}(\epsilon)\delta(\epsilon-\epsilon')\delta_{\sigma\sigma'} + G^X_{\delta j\ell,\sigma\bar{\sigma}}(\epsilon)\delta(\tilde{\epsilon}_\sigma-\epsilon')\delta_{\bar{\sigma}\sigma'} \quad (12)$$

to specify the spin diagonal and off-diagonal spin-flip effects. Note that the Green's functions possess the relation

$$G^r_{\delta j\ell,\bar{\sigma}\bar{\sigma}}(\tilde{\epsilon}_\sigma)\tilde{g}^r_{\delta j\ell,\sigma\sigma}(\epsilon) = G^r_{\delta j\ell,\sigma\sigma}(\epsilon)\tilde{g}^r_{\delta j\ell,\bar{\sigma}\bar{\sigma}}(\tilde{\epsilon}_\sigma). \quad (13)$$

This relation indicates the identity between the off-diagonal elements of Green's functions

$$G^X_{\delta j\ell,\bar{\sigma}\sigma}(\tilde{\epsilon}_\sigma) = G^X_{\delta j\ell,\sigma\bar{\sigma}}(\epsilon), \quad (14)$$

for $X \in \{r, a, <\}$. Substituting equation (12) into equation (8), we arrive at the time-dependent spin current components as

$$I_{\gamma,\sigma\sigma'}(t) = I_{\gamma,\sigma\sigma}\delta_{\sigma\sigma'} + I_{\gamma,\bar{\sigma}\sigma}e^{-i\lambda_\sigma\omega t}\delta_{\bar{\sigma}\sigma'}. \quad (15)$$

This presents that the spin diagonal transport components are independent on time, while the spin off-diagonal transport components oscillate with time.

The diagonal elements of the charge current is determined by summing up the spin-up and spin-down current elements as $I_\gamma = e(I_{\gamma,\uparrow\uparrow} + I_{\gamma,\downarrow\downarrow})$, while the $\mathbf{s}_z$ spin current component is given by the difference of spin-down and spin-up current components as $I^s_{\gamma,z} = \hbar(I_{\gamma,\downarrow\downarrow} - I_{\gamma,\uparrow\uparrow})/2$. The off-diagonal elements of the spin current components are associated with the $\mathbf{s}_x$ and $\mathbf{s}_y$ spin currents as $I^s_{\gamma,x} = \hbar(I_{\gamma,\uparrow\downarrow} + I_{\gamma,\downarrow\uparrow})/2$, and $I^s_{\gamma,y} = i(I_{\gamma,\downarrow\uparrow} - I_{\gamma,\uparrow\downarrow})\hbar/2$, respectively. This signifies that the spin currents $I^s_{\gamma,x}$ and $I^s_{\gamma,y}$ oscillate sinusoidally with time, and they are zero by taking time average. Therefore, only the $I^s_{\gamma,z}$ spin current component is nonzero by taking time average. The charge current and $\mathbf{s}_z$ component spin current are determined by the formula

$$I_{\gamma,\sigma\sigma} = -\frac{2}{h}Im\sum_{\delta\ell j}\int d\epsilon \Gamma^\sigma_{\gamma\delta,j\ell}(\epsilon)\Big[f_\gamma(\epsilon)G^r_{\delta j\ell,\sigma\sigma}(\epsilon) + \frac{1}{2}G^<_{\delta j\ell,\sigma\sigma}(\epsilon)\Big], \quad (16)$$

for $\gamma \in \{L, R, d\}$, which is proposed by Jauho, Wingreen, and Meir on considering the spin degenerate system in reference [24]. The line-widths of the γth lead and QD are determined by $\Gamma^\sigma_{\gamma\delta,j\ell}(\epsilon) = 2\pi\sum_k |R_{\gamma\delta,j\ell}(k)|^2\delta(\epsilon - E_{\gamma,k\sigma})$ for $\gamma \in \{L, R\}$, and $\Gamma^\sigma_{d\delta,j\ell}(\epsilon) = 2\pi\sum_{\ell'} |T^{\ell'\sigma}_{\delta,j\ell}|^2\delta(\epsilon - E_{d,\ell'\sigma})$ for $\gamma = d$. The DOS of the isolated QD is determined by the imaginary part of retarded Green's function of QD as $\rho_{d\sigma}(\epsilon) = -Im\sum_\ell g^r_{d,\ell\sigma}(\epsilon)/\pi$.

From equation (16), one can derive charge current and diagonal spin current elements associated with the following formula explicitly

$$I_{\gamma,\sigma\sigma} = \frac{1}{h}\sum_{\ell j\delta}\sum_{\gamma'}\int d\epsilon\Big\{T^{(1)\sigma\sigma}_{\delta j\ell,\gamma\gamma'}(\epsilon)[f_\gamma(\epsilon) - f_{\gamma'}(\epsilon)] + T^{(2)\sigma\bar{\sigma}}_{\delta j\ell,\gamma\gamma'}(\epsilon)[f_\gamma(\epsilon) - f_{\gamma'}(\tilde{\epsilon}_\sigma)]\Big\}, \quad (17)$$

for $\gamma, \gamma' \in \{L, R, d\}$. In the above current formula, we have defined the transmission coefficients as

$$T^{(1)\sigma\sigma}_{\delta j\ell,\gamma\gamma'}(\epsilon) = \Gamma^\sigma_{\gamma\delta,j\ell}(\epsilon)\Gamma^\sigma_{\gamma'\delta,j\ell}(\epsilon)|G^r_{\delta j\ell,\sigma\sigma}(\epsilon)|^2,$$
$$T^{(2)\sigma\sigma'}_{\delta j\ell,\gamma\gamma'}(\epsilon) = \Gamma^\sigma_{\gamma\delta,j\ell}(\epsilon)\Gamma^{\sigma'}_{\gamma'\delta,j\ell}(\tilde{\epsilon}_\sigma)\gamma^2(\theta) \times|\tilde{g}^r_{\delta j\ell,\bar{\sigma}\bar{\sigma}}(\tilde{\epsilon}_\sigma)|^2|G^r_{\delta j\ell,\sigma\sigma}(\epsilon)|^2. \quad (18)$$

The transmission coefficient $T^{(1)\sigma\sigma}_{\delta j\ell,\gamma\gamma'}(\epsilon)$ is symmetric about the terminals as $T^{(1)\sigma\sigma}_{\delta j\ell,\gamma\gamma'}(\epsilon) = T^{(1)\sigma\sigma}_{\delta j\ell,\gamma'\gamma}(\epsilon)$. Employing the symmetry relation equation (13), we have the symmetry

relation on the transmission coefficient as $T^{(2)\sigma\bar{\sigma}}_{\delta j\ell,\gamma\gamma'}(\epsilon) = T^{(2)\bar{\sigma}\sigma}_{\delta j\ell,\gamma'\gamma}(\tilde{\epsilon}_\sigma)$. This is equivalent to the case that the electron propagating with the spin-up and spin-down variables $\uparrow\downarrow$ changes to the spin state $\downarrow\uparrow$ due to the spin-flip effect as the electron tunnels from one lead to the other. This spin state transfer requires the absorption of photon energy $\lambda_\sigma\hbar\omega$. For our system, the self-energy of QD

$$\Sigma^r_{d\delta,j\ell\sigma}(\epsilon) = \beta^\sigma_{\delta j\ell}(\epsilon) - \frac{i}{2}\Gamma^\sigma_{d\delta,j\ell}(\epsilon) \tag{19}$$

depends on its energy levels intimately. The DOS of QD takes important role, and the wide-band limit is invalid. For the situation that the coupling strengths are independent on the energy levels between the TCN and QD $T^{\ell'\sigma}_{\delta,j\ell} = \mathcal{T}$, the self-energy $\Sigma^r_{d\delta,j\ell\sigma}(\epsilon)$ can be expressed by the DOS of QD through the line-width $\Gamma^\sigma_{d\delta,j\ell}(\epsilon) = 2\pi|\mathcal{T}|^2\rho_{d\sigma}(\epsilon)$, and the real part is settled by the principal value integral

$$\beta^\sigma_{\delta j\ell}(\epsilon) = |\mathcal{T}|^2 \int \rho_{\mathrm{d}\sigma}(\epsilon_1)\frac{\mathrm{d}\epsilon_1}{\epsilon - \epsilon_1}. \tag{20}$$

As the energy of electron satisfies the equation $w^\sigma_{\delta j\ell}(\epsilon) = \gamma^2(\theta)$, we achieve resonant transport through the TCN-QD system, where we have defined $w^\sigma_{\delta j\ell}(\epsilon) = [\epsilon - \varepsilon_{\delta j\ell,\sigma} - \beta^\sigma_{\delta j\ell}(\epsilon)][\tilde{\epsilon}_\sigma - \varepsilon_{\delta j\ell,\bar{\sigma}} - \beta^{\bar{\sigma}}_{\delta j\ell}(\tilde{\epsilon}_\sigma)] - \sum_{\gamma\gamma'}\Gamma^\sigma_{\gamma\delta,j\ell}(\epsilon)\Gamma^{\bar{\sigma}}_{\gamma'\delta,j\ell}(\tilde{\epsilon}_\sigma)/4$. The energy gap of an isolated single-wall carbon nanotube is determined by its concrete electronic structure, and it can be modified by the applied magnetic flux. By changing the magnetic flux, the metal-semiconductor phase transition occurs [26]. Similarly, as TCN is threaded with magnetic flux, energy gap will be modified by the applied magnetic flux, and the metal-semiconductor phase transition takes place [8]. In the numerical calculations, we find that conducting properties are different from the original isolated metallic TCN for the coupled TCN-QD systems, i.e., the isolated metallic TCN becomes semiconducting TCN-QD system, and the isolated semiconducting TCN becomes metallic TCN-QD system. These phase transitions are caused by the coupling of QD, by the magnetic flux threaded through the TCN, as well as by the rotating magnetic field.

2.1 Charge current

For the charge current, $I_\gamma = e\sum_\sigma I_{\gamma,\sigma\sigma}$, one observes the current conversation is satisfied by summing up all of the terminal currents to give $\sum_\gamma I_\gamma = 0$. This can be seen explicitly by changing $\gamma' \to \gamma$, and using the symmetry relation of $T^{(1)\sigma\sigma}_{\delta j\ell,\gamma\gamma'}(\epsilon)$ for the first term of equation (17). But for the second term of equation (17), summation contains spin-up and spin-down terms. However, we can shift the integration variable by letting $\epsilon \to \tilde{\epsilon}_\sigma$ in the second term of the spin-down current component. Employing the symmetry relation of $T^{(2)\sigma\bar{\sigma}}_{\delta j\ell,\gamma\gamma'}(\epsilon)$, and then changing the terminal notations as $\gamma\gamma' \to \gamma'\gamma$, one observes that the second term in equation (17) is exactly zero. Therefore, the conservation holds in our multi-terminal system. The charge current of γth terminal is given by the generalized spin-dependent Landauer-Büttiker formula

$$\begin{aligned} I_\gamma = \frac{e}{h}\sum_{\ell j\delta}\sum_{\gamma'}\int d\epsilon\Bigg\{ & \sum_\sigma T^{(1)\sigma\sigma}_{\delta j\ell,\gamma\gamma'}(\epsilon)[f_\gamma(\epsilon) - f_{\gamma'}(\epsilon)] \\ & + T^{(2)\uparrow\downarrow}_{\delta j\ell,\gamma\gamma'}(\epsilon)[f_\gamma(\epsilon) - f_{\gamma'}(\tilde{\epsilon}_\uparrow)] \\ & + T^{(2)\uparrow\downarrow}_{\delta j\ell,\gamma'\gamma}(\epsilon)[f_\gamma(\tilde{\epsilon}_\uparrow) - f_{\gamma'}(\epsilon)]\Bigg\}. \end{aligned} \tag{21}$$

We observe that the charge current is nonzero in the presence of rotating magnetic field even if $\mu_\gamma = \mu_{\gamma'}$, (for $\gamma \neq \gamma'$), since $T^{(2)\uparrow\downarrow}_{\delta j\ell,\gamma\gamma'}(\epsilon) \neq T^{(2)\uparrow\downarrow}_{\delta j\ell,\gamma'\gamma}(\epsilon)$ generally. This is equivalent to the case that the rotating magnetic field causes spin-flip, and it pumps the electrons to different terminals. The different properties of terminals cause net charge current. If we replace QD as a normal metal terminal, and take the wide-band limit in the terminals, i.e., $\Sigma^r_{\gamma\delta,j\ell\sigma}(\epsilon) = -i\Gamma_\gamma/2$, the line-widths are independent on energy levels, and the charge current is zero $I_\gamma = 0$ as $\mu_\gamma = \mu_{\gamma'}$ [17]. The photon pumping effect can be observed explicitly at zero temperature, where the Fermi distribution function becomes step function. We denote the chemical differences as $\mu_L - \mu_R = eV$ and $\mu_L - \mu_d = eV_d$. In order to present main physical feature of spin-flip transport and photon pumping effect, we keep $\mu_L = \mu_d$ and take μ_R as the measurement point by setting $\mu_R = 0$. Therefore, the charge current tunnelling from the left terminal to the central region is determined by the formula

$$\begin{aligned} I_L = \frac{e}{h}\sum_{\ell j\delta}\Bigg\{ & \int_{\hbar\omega}^{eV} d\epsilon[T^{(2)\uparrow\downarrow}_{\delta j\ell,LR}(\epsilon) + T^{(2)\uparrow\downarrow}_{\delta j\ell,Ld}(\epsilon)] \\ & + \int_0^{eV+\hbar\omega} d\epsilon[T^{(2)\uparrow\downarrow}_{\delta j\ell,RL}(\epsilon) + T^{(2)\uparrow\downarrow}_{\delta j\ell,dL}(\epsilon)] \\ & + \sum_\sigma\int_0^{eV} d\epsilon T^{(1)\sigma\sigma}_{\delta j\ell,LR}(\epsilon)\Bigg\}. \end{aligned} \tag{22}$$

As the source-drain bias $eV = 0$, by taking wide-band limit for the left and right leads, we obtain the pumping charge current

$$I_L = \frac{e}{h}\sum_{\ell j\delta}\int_0^{\hbar\omega} d\epsilon\left[T^{(2)\uparrow\downarrow}_{\delta j\ell,dL}(\epsilon) - T^{(2)\uparrow\downarrow}_{\delta j\ell,Ld}(\epsilon)\right]. \tag{23}$$

This pumping charge current is expressed in explicit form by substituting the transmission coefficient shown in equation (18) to be associated with the quantity determined by the difference of line-width of QD as $\widetilde{\Gamma}_{\delta,j\ell}(\epsilon) = \Gamma^\uparrow_{d\delta,j\ell}(\epsilon) - \Gamma^\downarrow_{d\delta,j\ell}(\tilde{\epsilon}_\uparrow)$. The difference of line-width $\widetilde{\Gamma}_{d\delta,j\ell}(\epsilon)$ is nonzero generally, since $\Gamma^\sigma_{d\delta,j\ell}(\epsilon)$ is dependent on spin variable, and it is modified by the photon energy $\lambda_\sigma\hbar\omega$. However, the numerical calculation shows that the pumped charge current is very small except several definite points of frequency.

2.2 Spin current

We consider the zero biased terminals $\mu_{\gamma'} = \mu_\gamma$, where $\gamma, \gamma' \in \{L, R, d\}$, in order to investigate the spin current induced by the rotating magnetic field. The $\mathbf{s}_z$ spin current component in the γth lead is determined by employing equation (17) to give

$$I^s_{\gamma,z} = \frac{1}{4\pi}\sum_{\ell j\delta}\sum_{\gamma'}\int d\epsilon\Big\{T^{(2)\uparrow\downarrow}_{\delta j\ell,\gamma'\gamma}(\epsilon)[f_\gamma(\tilde{\epsilon}_\uparrow) - f_{\gamma'}(\epsilon)] - T^{(2)\uparrow\downarrow}_{\delta j\ell,\gamma\gamma'}(\epsilon)[f_\gamma(\epsilon) - f_{\gamma'}(\tilde{\epsilon}_\uparrow)]\Big\}. \quad (24)$$

The zero temperature $\mathbf{s}_z$ spin current component takes the form as follows in the wide-band limit for the left and right leads as

$$I^s_{L,z} = \frac{1}{2\pi}\sum_{\ell j\delta}\int_0^{\hbar\omega} d\epsilon\Gamma_L\widetilde{\Gamma}_{\delta,j\ell}(\epsilon)\gamma^2(\theta) \times |\tilde{g}^r_{\delta j\ell,\downarrow\downarrow}(\tilde{\epsilon}_\uparrow)|^2|G^r_{\delta j\ell,\uparrow\uparrow}(\epsilon)|^2, \quad (25)$$

where $\widetilde{\Gamma}_{\delta,j\ell}(\epsilon)$ is defined by the summation of the terminal line-widths as $\widetilde{\Gamma}_{\delta,j\ell}(\epsilon) = \Gamma_L + \Gamma_R + \frac{1}{2}[\Gamma^\uparrow_{d\delta,j\ell}(\epsilon) + \Gamma^\downarrow_{d\delta,j\ell}(\tilde{\epsilon}_\uparrow)]$. This formula shows that the rotating magnetic field may generate spin current as the photon energy of the system satisfies the condition as $\hbar\omega > E_g(\phi)/2$, where $E_g(\phi)$ is the energy gap of TCN-QD system.

The $\mathbf{s}_\mathrm{x}$ and $\mathbf{s}_\mathrm{y}$ components of spin current are determined by

$$I^s_{\gamma,x} = I_{\gamma(1)}\sin(\omega t) + I_{\gamma(2)}\cos(\omega t), \quad (26)$$

$$I^s_{\gamma,y} = I_{\gamma(2)}\sin(\omega t) - I_{\gamma(1)}\cos(\omega t), \quad (27)$$

where the magnitudes of the spin current above are determined by the off-diagonal Green's functions. The quantity $I_{\gamma(2)}$ is a complex function which contains real and imaginary parts. The imaginary part of the spin current is induced by the polarization procedure due to the spin flip, and it can be referred as the polarization spin current. The real part of the spin current is the tunnelling spin current which consumes energy in order to produce work. The spin currents $I^s_{\gamma,x}$ and $I^s_{\gamma,y}$ evolve with time possessing $\pi/2$ phase difference, i.e., $I^s_{\gamma,y}(\omega t + \pi/2) = I^s_{\gamma,x}(\omega t)$.

3 Numerical calculation

We consider the wide-band limit for the normal metal leads, and we assume that the tunnelling electrons possess equal coupling strength between the leads and TCN. This means the line-widths of leads are energy-independent $\Gamma_L = \Gamma_R = \Gamma$, which presents main behaviors of mesoscopic transport. In the numerical calculations, we take parameters as $\Gamma = 3.033$ meV, $\mathcal{T} = 3.033$ meV, and $\mu B_0 = 0.05\gamma_0$,($B_0 \approx 2.6 \times 10^3$ T). The QD is assumed to possess multiple levels with equal level spacing $\Delta E_{d\ell} = \ell\Delta_0$, ($\ell = 0, \pm1, \pm, 2, ...\mathcal{N}$), where $\Delta_0 = 0.025\gamma_0$, and $\nu = \gamma_0/h \approx 7.36^{14}$ Hz. We only deal with the zero-temperature systems which can provide obvious quantum effects. We drop the terminal label $\gamma = L$ in the following figures for current labelling.

Figure 1 shows the differential conductance with respect to the source-drain bias eV for different TCN-QD systems. We set the external parameters ϕ, V_g, B_2 to be zero to study the conductance structure related to the material and applied rotating magnetic field $\mathbf{B}_0$. Diagram (a) displays the conductance structure of the type II (7, 7; −160, 160) TCN in the presence of a rotating magnetic field. For the isolated type II TCN, it exhibits semiconducting properties in the absence of external field. However, for our compound system, the DOS of QD contributes additional levels for electron to tunnel. Further more, the rotating magnetic field also induces novel levels due to the spin splitting and photon absorption procedures. This is equivalent to the situation that the system experiences a semiconductor-metal phase transition. Therefore, one observes that the mesoscopic system exhibits metal feature of resonant differential conductance. Diagram (b) is the differential conductance of the type III TCN system as $\hbar\omega = 0$. The system displays the semiconducting behavior with large energy gap $E_g \approx 1.21$ eV. This indicates that the type III TCN system is a semiconductor even if it is coupled by a QD with multi-levels as $eV_g = 0, \phi = 0$, and $B_2 = 0$. This behavior is caused due to the large energy gap, and the DOS of QD can not induce additional energy levels to bridge the energy gap. Diagrams (c) and (d) are associated with the type I (7, 7; −159, 159) TCN system. One observes that as $\hbar\omega = 0$, the system displays the semiconducting structure with narrow energy gap $E_g \approx 60$ meV. This energy gap is caused by the coupling of QD, since the isolated TCN in the absence of external magnetic field possesses the metallic feature. The conductance resonant peaks are modified as the photon energy is nonzero shown in diagram (d). The suppression and enhancement of resonant peaks are observed due to the rotating magnetic field. However, it still exhibits the semiconducting behavior since the conductance is zero at $eV = 0$.

We present the differential conductance versus the photon energy $\hbar\omega$ of the rotating magnetic field in Figure 2. The resonant structures of conductance are observed, which is strongly associated with the DOS of the coupled system. Diagram (a) represents the metallic feature with zero energy gap $E_g = 0$ for the type II (7, 7; −160, 160) TCN system, and the photon absorption can cause pumping current even if $V = 0$. In addition to the nature of microstructure of the TCN-QD system, the differential conductance is contributed intimately by the photon absorption and spin-flip effects originated from the rotating magnetic field. We depict the differential conductance of the type III (7,0;-160,320) TCN system in diagram (b). The semiconducting behavior of the compound system is still observed due to measuring the conductance versus applied photon energy $\hbar\omega$. The conductance is non-zero only as the photon energy is large enough as $\hbar\omega > 0.667$ eV.

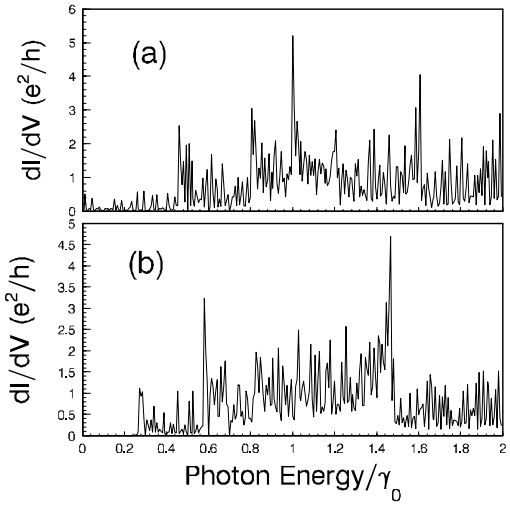

Fig. 2. The differential conductance dI/dV versus photon energy $\hbar\omega$ of the rotating magnetic field. The parameters are chosen as $\phi = 0$, $V_g = 0, B_2 = 0, \theta = \pi/3$, $V = 0$, $\mathcal{N} = 30$. Diagrams (a) and (b) are associated with the (7, 7; −160, 160) and (7, 0; −160, 320) TCNs, respectively.

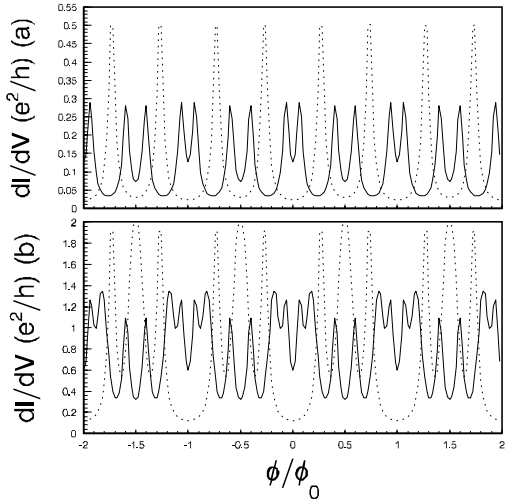

Fig. 3. The differential conductance dI/dV versus magnetic flux ϕ. The parameters are chosen as $V_g = 0, B_2 = 0, \theta = \pi/3, \hbar\omega = 0.01\gamma_0, \mathcal{N} = 30$. The dotted and solid curves are associated with the (7, 7; −159, 159) and (7, 7; −160, 160) TCNs. Diagrams (a) and (b) are related to the conductance at $V = 0$ and $eV = 0.01\gamma_0$, respectively.

We display the oscillation of differential conductance with respect to the magnetic flux ϕ in Figure 3, which is associated with the Aharonov-Bohm effect. The dotted and solid curves are related to the type I (7, 7; −159, 159) and type II (7, 7; −160, 160) TCNs, respectively. The periodic oscillation with the period ϕ_0 is observed, and the conductance satisfies the relation of even function of ϕ as usual. However, the magnitude and oscillation structures are strongly dependent on the detailed structure of TCN and the applied source-drain voltage V. As $V = 0$, the magnitude of dI/dV for the (7, 7; −160, 160) TCN-QD system is about 0.3 e^2/h, and there contains four resonant peaks in a period shown in diagram (a). But for the (7, 7; −159, 159) TCN-QD system, one observes that the magnitude of conductance is 0.5 e^2/h, while there exist two resonant peaks in a period. The oscillation structures are quite different when the source-drain bias is applied as $eV = 0.01\gamma_0$ shown in diagram (b). The cluster oscillations are exhibited to contain three peaks in a period for the type I TCN system, but it contains six peaks in a cluster for the type II TCN system.

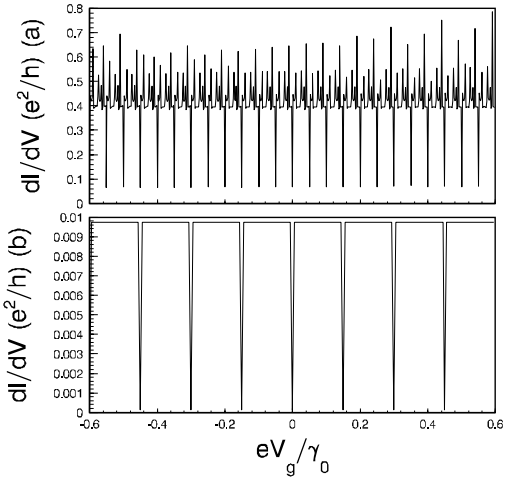

Fig. 4. The differential conductance dI/dV versus gate voltage V_g. The parameters are chosen as $\phi = 0, B_2 = 0, \theta = \pi/3, V = 0, \mathcal{N} = 30$. Diagram (a) corresponds to the (7, 7; −160, 160) TCN as $\hbar\omega = 0.01\gamma_0$. Diagram (b) corresponds to the (7, 0; −160, 320) TCN as $\hbar\omega = 0$.

The differential conductance is adjusted by the gate voltage V_g shown in Figure 4 for the type II (7, 7; −160, 160) and type III (7, 0; −160, 320) TCN-QD systems. The Fano type of multi-resonant behaviors are displayed in diagram (a), and the reverse resonance structure is observed in diagram (b). For the differential conductance of the type II (7, 7; −160, 160) TCN-QD, several resonant peaks with different heights are located on each of the conductance plateaus. The plateau conductance possess the height as about 0.4 e^2/h and the width $eV_g = 0.05\gamma_0$. This width is not equal to the level spacing of the QD as $\Delta_0 = 0.025\gamma_0$ stated before. This signifies that the microstructure of the TCN-QD system possesses its specific transport properties different from the separated subsystems. The rotating magnetic field induces asymmetric tunnelling behaviors due to the spin-flip effect, and the charge conductance is strongly affected by it. For the type III (7, 0; −160, 320) TCN-QD system, the differential conductance is suppressed completely from about 0.01 e^2/h at definite values of gate voltage. This implies that for the semiconducting system, the conductance exhibits constant value in large regimes of the gate voltage. The width of each conductance rectangle is about 0.15 γ_0. The conductance is naturally originated from the combination of compound system.

As the QD is applied with Zeeman field $\mathbf{B}_2$, the levels of QD is split to form non-degenerate QD system, and the electronic transport for the coupled TCN-QD system is

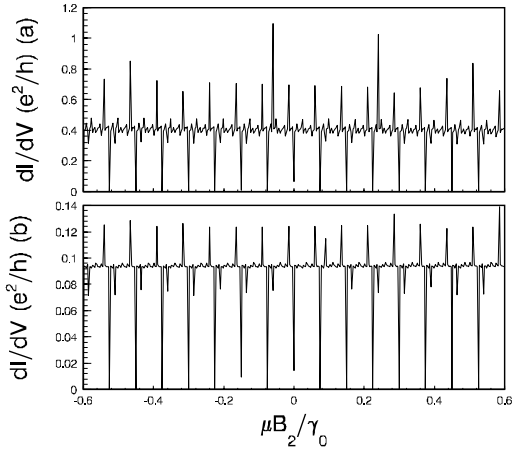

Fig. 5. The differential conductance dI/dV versus the Zeeman energy μB_2. The parameters are chosen as $\phi = 0, \theta = \pi/3, V = 0, V_g = 0, \hbar\omega = 0.01\gamma_0, \mathcal{N}$=30. Diagrams (a) and (b) correspond to the (7, 7; −160, 160) and (7, 7; −159, 159) TCNs, respectively.

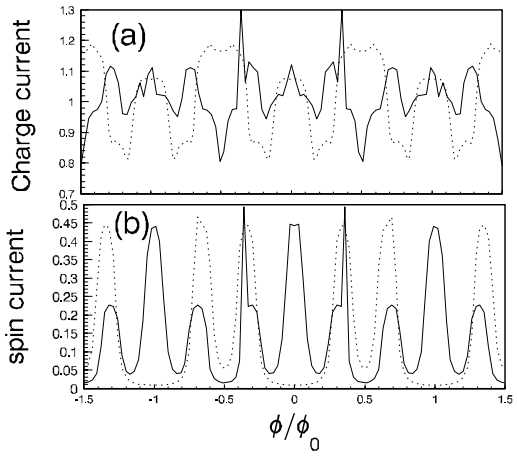

Fig. 6. The charge and spin currents versus magnetic flux ϕ. The parameters are chosen as $\theta = \pi/3, B_2 = 0, V_g = 0, \hbar\omega = 0.01\gamma_0, \mathcal{N} = 2$. Diagram (a) is the charge current scaled by $e\Gamma/h$ as the source-drain bias $eV = 0.03\gamma_0$, while diagram (b) is the spin current I_z^s scaled by $10^{-2}\Gamma/(2\pi)$ in the absence of the source-drain bias $eV = 0$. The solid and dotted curves are associated with (7, 7; −74, 74) and (7, 7; −75, 75) TCNs, respectively.

contributed by the spin-flip TCN and spin split QD subsystems, as well as by the combination of the compound structure. We can control the charge transport by varying the magnitude of $\mathbf{B}_2$ to obtain desired conductance exhibited in Figure 5 for the type I and II TCN-QD systems. The Fano resonant conductance structures are observed for the two systems associated with (7, 7; −160, 160) and (7, 7; −159, 159)TCNs shown in diagrams (a) and (b), respectively. The magnitudes of the type II conductance fluctuates around 0.4 e^2/h, and it can be suppressed completely by varying the Zeeman field $\mathbf{B}_2$. But for the type I TCN, the maximum magnitude of conductance is 0.12 e^2/h, and the conductance fluctuates around 0.09 e^2/h. The conductance of this type system can also be suppressed completely by varying the Zeeman field $\mathbf{B}_2$. One can see that the suppressions of the conductance takes place with the separation $\mu B_2 = 0.075\gamma_0$ for both of the systems. Compared with the conductance shown in Figure 4, we find that the conductance possesses different controlling behaviors with respect to eV_g and μB_2.

Figure 6 shows the charge and spin currents I and I_z^s in the presence of rotating magnetic field with photon energy $\hbar\omega = 0.01\gamma_0$. The charge current is depicted as the source-drain bias $eV = 0.03\gamma_0$, and the spin current is shown as $eV = 0$. The charge and spin currents oscillate with ϕ showing different oscillation structures for the type I and II TCN-QD systems. The main peaks and valleys of the currents are located at the same place for the two systems, and cluster-peak oscillation structures are seen. For the charge current, one observes that the current of the type I TCN-QD system varies with ϕ smoothly. The larger oscillation wave is embedded with smaller peak oscillation, while for the type II TCN-QD system, multi-peaks are located on the main current oscillation plateaus. The spin current oscillates also smoothly for the type I TCN-QD system with two peaks appearing in a period ϕ_0. For the type II TCN-QD system, a main spin current peak is accompanied with two side peaks.

Figure 7 exhibits the spin current I_z^s versus the photon energy $\hbar\omega$ of rotating magnetic field. The solid curve is related to type II (7, 7; −74, 74) TCN-QD system, which possesses metal-like behavior since the spin current occurs in the presence of nonzero photon energy. This signifies that the spin current can be induced by applying a rotating magnetic field. A step appears at about $0.035\gamma_0$, and a peak at $0.06\gamma_0$. As the photon energy increases to $0.08\gamma_0$, the spin current increases rapidly. The dotted curve represents the spin current of type I (7, 7; −75, 75) TCN-QD system which contains energy threshold $E_g/2 \approx 0.05\gamma_0$. In order to obtain spin current I_z^s obviously, we must apply the rotating magnetic field with photon energy $\hbar\omega > 0.05\gamma_0$. This procedure is equivalent to the case that the electrons tunnelling from the electrodes absorbing photon energy which is greater than 0.152 eV can overcome the energy threshold to form spin current. The resonant peak occurred at $\hbar\omega \approx 0.6\gamma_0$ reflects the nonlinear quantum structure.

The spin transport is strongly related to the tilt angle of magnetic field with respect to the z-axis stated as θ. It is directly seen that as $\theta = n\pi$, (n = 0, 1, 2, ...), the spin-flip effect disappears due to $\gamma(\theta) = 0$ at these points. This means that the spin current is zero as $\theta = n\pi$. However, we can not observe directly the variation of spin current associated with θ in the regime $0 < |\theta| < \pi$ from the formulas, since the spin transport is dependent on θ completely related to the detailed microstructure of the system. We display the spin current I_z^s versus θ in Figure 8 to show the variation of spin current. Two resonant peaks emerge at about $\theta = \pm 0.2\pi$ for both of the (7, 7; −74, 74) and (7, 7; −75, 75) TCN-QD systems. But for the (7, 7; −75, 75) TCN-QD system, there exhibits two side peaks at about $\theta = \pm 0.35\pi$. The main peaks of this type system are suppressed by comparing with the type II TCN-QD system.

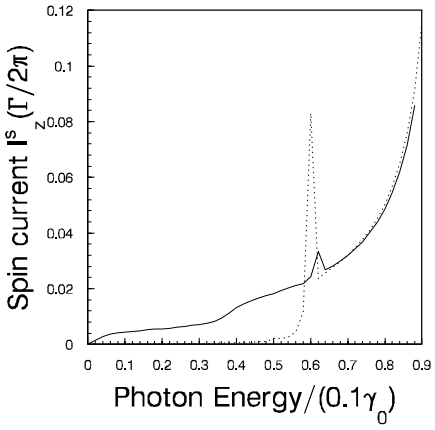

Fig. 7. The spin current I_z^s versus photon energy $\hbar\omega$. The parameters are chosen as $\theta = \pi/3, B_2 = 0, V_g = 0, \phi = 0, V = 0, \mathcal{N} = 2$. The solid and dotted curves are related to the (7, 7; −74, 74) and (7, 7; −75, 75) TCNs, respectively.

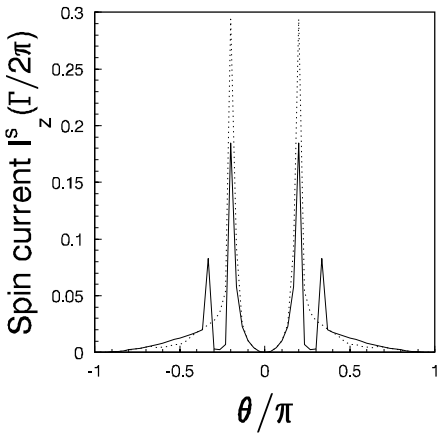

Fig. 8. The spin current I_z^s versus the magnetic tilt angle θ. The parameters are chosen as $V_g = 0, B_2 = 0, V = 0, \phi = 0, \hbar\omega = 0.06\gamma_0, \mathcal{N} = 2$. The dotted and solid curves are related to the (7, 7; −74, 74) and (7, 7; −75, 75) TCNs, respectively.

This also indicates that the type II TCN-QD system can provide larger spin current, while the type I TCN-QD system can provide more detailed transport behaviors.

4 Concluding remark

The microstructure of TCN-QD system possesses its specific transport properties different from the separated sub-systems. The differential conductance is contributed intimately by the photon absorption and spin-flip effects originated from the rotating magnetic field. The magnitude and oscillation structures are strongly dependent on the detailed structure of TCN and the applied source-drain voltage V. The Fano type of multi-resonant behaviors are displayed in the conductance structures by adjusting the gate voltage V_g and the Zeeman field $\mathbf{B}_2$ applied on the QD. The reverse resonance structure versus gate voltage is also exhibited in the large energy gap semiconducting system. The rotating magnetic field induces asymmetric tunnelling behaviors due to the spin-flip effect, and the charge conductance is strongly affected by it. The conductance possesses different controlling behaviors with respect to eV_g and μB_2. The spin transport is strongly related to the tilt angle of magnetic field θ. The spin current displays quite different structures compared with different TCN-QD systems.

This work was supported by a RGC grant from the SAR Government of Hong Kong under Grant No. HKU 7044/05P, by the National Natural Science Foundation of China under the Grant No. 10375007.

References

1. K. Tsukagoshi, B.W. Alphenaar, H. Ago, Nature (London) **401**, 572 (1999)
2. A.F. Morpurgo, J. Kong, C.M. Marcus, H. Dai, Science **286**, 263 (1999)
3. H. Mehrez, J. Taylor, H. Guo, J. Wang, C. Roland, Phys. Rev. Lett. **84**, 2682 (2000)
4. B.I. Dunlap, Phys. Rev. B **46**, 1933 (1992)
5. S. Itoh, S. Ihara, J. Kitakami, Phys. Rev. B **47**, 1703 (1993); S. Itoh, S. Ihara, J. Kitakami, Phys. Rev. B **47**, 12908 (1993)
6. R.C. Haddon, Nature (London) **388**, 31 (1997)
7. R. Martel, H.R. Shea, Ph. Avouris, Nature (London) **398**, 299 (1999); H.R. Shea, R. Martel, Ph. Avouris, Phys. Rev. Lett. **84**, 4441 (2000)
8. M.F. Lin, D.S. Chuu, Phys. Rev. B **57**, 6731 (1998); R. Saito, G. Dresselhaus, M.S. Dresselhaus, *Physical Properties of Carbon Nanotubes* (Imperial College Press, London, 1998)
9. H.K. Zhao, Phys. Lett. A **310**, 207 (2003); H.K. Zhao, Phys. Lett. A **317**, 329 (2003)
10. H.K. Zhao, Phys. Lett. A **308**, 226 (2003); H.K. Zhao, Eur. Phys. J. B **33**, 365 (2003)
11. H.K. Zhao, J. Wang, Phys. Lett. A **325**, 285 (2004); H.K. Zhao, J. Wang, Eur. Phys. J. B **40**, 93 (2004)
12. S. Datta, B. Das, Appl. Phys. Lett. **56**, 665 (1990)
13. S.A. Wolf et al., Science **294**, 1488 (2001); R. Fiederling et al., Nature (London) **402**, 787 (1999)
14. G.A. Prinz, Science **282**, 1660 (1998); Y. Ohno et al., Nature (London) **402**, 790 (1999)
15. A. Brataas, Y. Tserkovnyak, G.E.W. Bauer, B. Halperin, Phys. Rev. B **66**, 060404 (2002)
16. Q.F. Sun, H. Guo, J. Wang, Phys. Rev. Lett. **90**, 25830 (2003)
17. B. Wang, J. Wang, H. Guo, Phys. Rev. B **67**, 092408 (2003)
18. H.K. Zhao, J. Wang, Eur. Phys. J. B **44**, 93 (2005)
19. H.K. Zhao, Q. Wang, Phys. Lett. A **338**, 425 (2005)
20. H.K. Zhao, L.N. Zhao, Eur. Phys. J. B **47**, 295 (2005)
21. M. Büttiker, C.A. Stafford, Phys. Rev. Lett. **76**, 495 (1996)
22. P. Zhang, Q.K. Xie, X.C. Xie, Phys. Rev. Lett. **91**, 196602 (2003)
23. T. Ando, Semicond. Sci. Technol. **15**, R13 (2000)
24. A.P. Jauho, N.S. Wingreen, Y. Meir, Phys. Rev. B **50**, 5528 (1994)
25. H.K. Zhao, Z. Phys. B **102**, 415 (1997); H.K. Zhao, Phys. Lett. A **226**, 105 (1997); H.K. Zhao, Phys. Rev. B **63**, 205327 (2001)
26. J.P. Lu, Phys. Rev. Lett. **74**, 1123 (1995)